Near-infrared spectroscopic monitoring of WR 140 during the 2001 periastron passage

Watson P. Varricatt,[1]★ P. M. Williams[2]★ and N. M. Ashok[3]★

[1]*Joint Astronomy Centre, 660 N. A‘ohōkū Place, Hilo, Hawaii 96720, USA*
[2]*Institute for Astronomy, University of Edinburgh, Royal Observatory, Edinburgh EH9 3HJ*
[3]*Physical Research Laboratory, Navrangpura, Ahmedabad 380009, India*

ABSTRACT

We present new spectra of WR 140 (HD 193793) in the *JHK* bands, with some covering the 1.083-μm He I emission line at higher resolution, observed between 2000 October and 2003 May to cover its 2001 periastron passage and maximum colliding-wind activity. The WC7 + O4–5 spectroscopic binary WR 140 is the prototype of colliding-wind, episodic dust-making Wolf–Rayet systems, which also show strong variations in radio and X-ray emission. The *JHK* spectra showed changes in continuum and in the equivalent widths of the WC emission lines, consistent with the formation of dust, starting between 2001 January 3 and March 26 (orbital phases 0.989 and 0.017) and its subsequent fading and cooling. The 1.083-μm He I line has a P Cygni profile, which showed variations in both absorption and emission components as WR 140 went through periastron passage. The variation of the absorption component of the profile yielded tight constraints on the geometry of the wind-collision region, giving $\theta = 50° \pm 8°$ for the opening semi-angle of the interaction region 'cone', indicating a wind-momentum ratio $(\dot{M}v_\infty)_O/(\dot{M}v_\infty)_{WR} = 0.10$, about three times larger than previously believed. As the system approached periastron, the normally flat-topped emission component of the 1.083-μm line profile showed the appearance of a significant subpeak. The movement of the subpeak across the profile was seen to be consistent with its formation in wind material flowing along the contact discontinuity between the WC7 and O4–5 stellar winds and the changing orientation of the colliding-wind region as the stars moved in their orbits. The flux carried in the subpeak was significant, exceeding the X-ray fluxes measured at previous periastron passages. This additional source of radiative cooling of the shock-heated gas probably causes it to depart from being adiabatic around periastron passage, thereby accounting for the departure of the X-ray flux from its previously expected $1/d$ dependence.

Key words: binaries: spectroscopic – circumstellar matter – stars: individual: WR 140 – stars: winds, outflows – stars: Wolf–Rayet.

1 INTRODUCTION

Stars with $M_* \geqslant 30\ \mathrm{M_\odot}$ go through a Wolf–Rayet (WR) phase in their evolution, during which they undergo large-scale mass loss ($\dot{M} \sim 10^{-5}\ \mathrm{M_\odot\ yr^{-1}}$). Consequently they display broad emission-line spectra and large infrared (IR) excesses originating in their accelerated stellar winds (wind terminal velocity $v_\infty = 750$–5000 km s^{-1}). They are post-main-sequence stars that have lost most of their hydrogen envelopes through stellar winds in the pre-WR stage. Based on the emission lines seen, they are classified as WN stars

(lines of He, N and H), WC and WO stars (lines of He, C and O). Late WC stars (WC7–9) show evidence of circumstellar dust, mainly of amorphous carbon (Williams 1995). Some of them are persistent dust-makers, which show continuous dust formation, and others are episodic dust-makers, where we see periodic rises in their IR flux due to episodic formation of dust. It is believed, now, that episodic dust-making WC stars are massive binary systems in which the stellar winds of two massive stars interact. WR 140 (HD 193793) is the prototype of colliding-wind, episodic dust-forming WC stars (Williams 1995).

From the photometry of the infrared maxima in 1985 and 1977 and earlier data, Williams et al. (1987) found that the occurrence of the IR maxima and the dust formation were periodic and derived a period of 7.9 yr. Studying the existing radial velocity data, from which

★E-mail: w.varricatt@jach.hawaii.edu (WPV); pmw@roe.ac.uk (PMW); ashok@prl.ernet.in (NMA)

no orbit had previously been derived, they showed that WR 140 was indeed a spectroscopic binary with high eccentricity. This was extended to a multiwavelength study, including 1.65–12.6 µm light curves, radio and X-ray data by Williams et al. (1990, hereafter W90), who derived a photometric period $P = 2900 \pm 10$ d (7.94 yr) and a spectroscopic orbit from published radial velocities giving elements $e = 0.84 \pm 0.04$, $\omega = 32° \pm 8°$ and $T_0 = $ JD244 6160 $\pm$ 29 (1985.26 $\pm$ 0.08). The system formed dust for about four months, 4 per cent of the period, during periastron passage. This is perhaps one of the least well understood of the phenomena shown by WR 140.

The most recent periastron passage and dust formation episode occurred in early 2001, for which a multiwavelength observing campaign was planned and undertaken.

Marchenko et al. (2003) carried out optical photometric and spectroscopic observations and derived a spectroscopic period $P = 2899 \pm 1.3$ d, in excellent agreement with the photometric period and new orbital elements, $e = 0.881 \pm 0.005$, $\omega = 46.7° \pm 1.6°$ and $T_0 = $ JD244 6147.4 $\pm$ 3.7, which we use in this paper. They found that, at phases very close to periastron, the profiles of the 5696-Å C III and 5876-Å He I lines developed extra emission components at their 'blue' ends that rapidly moved to the red.

Panov & Dinko (2002) observed a minimum in *UBV* photometric bands in 2001 June (phase = 0.038–0.046). This minimum was observed at the same phase, but deeper than the optical minimum observed in 1993 (Panov, Altmann & Seggewiss 2000). By 2001 July, the optical light almost reached the pre-eclipse level. They interpreted this eclipse-like phenomenon as due to the carbon dust envelope, the formation of which was triggered at the periastron passage. The difference in the rising part of the eclipse light curves of 1993 and 2001 could be due to the differences in clumping in the expanding dust shell from cycle to cycle. Aperture-masking interferometric observations by Monnier, Tuthill & Danchi (2002) using the Keck Telescope showed the first direct images of dust in WR 140. Comparison of their pre-periastron observation in 1999 June and post-periastron observation in 2001 July at 2.2 µm shows expanding clumpy dust. They resolved five clumps in the shell, expanding with velocities 0.46–1.29 mas d^{-1}.

The programme of near-IR spectroscopy described in the present paper was undertaken to search for changes in the IR line spectrum, particularly the profile of the He I line at 1.083 µm, around the time of maximum colliding-wind activity. Previous 1-µm and *JHK* spectroscopy (e.g. Vreux, Andrillat & Biémont 1990; Eenens, Williams & Wade 1991), and observations of the 1.083-µm He I line profile (Eenens & Williams 1994), were made at phases far from periastron. In each observation, the 1.083-µm emission-line profile showed a flat top, characteristic of formation in the asymptotic region of the Wolf–Rayet wind, with no evidence of a subpeak, which could be formed in a wind-collision region (Stevens & Howarth, 1999). Nevertheless, given the very high eccentricity of the binary system and short duration of maximum colliding-wind activity such as dust formation, we considered it worth reobserving the 1.083-µm profile as close to the periastron as possible.

2 OBSERVATIONS

We observed near-IR spectra of WR 140 using the 3.8-m United Kingdom Infrared Telescope (UKIRT) on Mauna Kea, Hawaii, and the 1.2-m Mt Abu Infrared Telescope, India. The UKIRT observations were made using the Cooled Grating Spectrometer (CGS4) and the UKIRT 1–5 µm Imager Spectrometer (UIST), while the Mt Abu observations were made using a liquid-nitrogen-cooled NIC-

MOS array imager and spectrometer. We observed WR 140 from 2000 October to 2003 May, covering the periastron passage expected in 2001 February. No observations were possible during January and February since WR 140 was not available at night. From 2000 October to 2001 March, the He I line at 1.083 µm was observed using CGS4 and the 150 lines mm^{-1} grating at a spectral resolution of ~4700, after which this grating was not available for observations. In 2003 May, this line was again observed using UIST with the short_*J* grism, which gives a spectral resolution of 3000 with a two-pixel slit. From 2001 March, observations were performed in *J*, *H* and *K* bands using CGS4 and the 40 lines mm^{-1} grating, which gives a resolution of 800 in the *J* band in the second order and 400 in the *H* and *K* bands in the first order. Observations using the Mt Abu spectrometer were done in the *JHK* bands at a resolution of ~1000 in 1998 May and from 2000 December to 2001 April. Because of decreasing transmission of the blocking filter towards shorter wavelengths, the signal-to-noise ratio (S/N) of the *J* spectra observed by the Mt Abu spectrometer decreases towards 1.083 µm. However, the line profile variations of the He I line are clearly seen. Table 1 gives details of the spectroscopic observations. In the last column, *d* refers to the separation between the O star and the WC star at any epoch of observation and *a* refers to the semimajor axis of the relative orbit with the WC star at one of the foci.

3 THE *JHK*-BAND SPECTRA

Figs 1 and 2 show the *J*-band spectra observed from Mauna Kea and Mt Abu respectively. One of the Mt Abu spectra (2001 January 2) is also shown in Fig. 1 along with the *J* spectra of later epochs from Mauna Kea for comparison of the continuum. Fig. 3 shows the *H* and *K* spectra. The gap in the spectra is the region where the telluric absorption makes the atmospheric transmission poor. Each spectrum is labelled with the date of observation and orbital phase of the binary system. Fig. 4 shows the observed, flux-calibrated spectra observed on 2003 May 24 using UKIRT and UIST. The data were flux-calibrated using photometry from Mt Abu Observatory on 2003 June 5 and 12, which gave average magnitudes of $J = 5.61 \pm 0.07$ and $H = 5.34 \pm 0.07$ respectively. Spectra of 2003 May 24 are dereddened assuming $E(B - V) = 0.6$ (Eenens & Williams 1992) and the equivalent widths (EWs) of the spectral lines are determined fitting Gaussian profiles. Multiple Gaussians are fitted when the lines are blended. Table 2 lists the spectral lines identified and their fluxes and equivalent widths, estimated from the dereddened spectra. The 1σ errors are given in brackets against the estimated values. The main source of errors is from the definition of the continuum. The error estimates are done from multiple attempts of the fits. Line identifications are done in comparison with the near-IR spectra of WR 140 and the identifications of Eenens & Williams (1992) and from the atomic line list of Peter A. M. van Hoof.[1] For the 1.083-µm He I line, since the line was flat-topped, multiple lines were fitted to estimate the line flux and EW. A comparison of the line fluxes with those of Eenens & Williams (1992) (spectra taken in 1988 July, phase = 0.41) shows that the line fluxes of most of the prominent lines match well, implying that the wind properties of the system are very much repeatable.

As a measure of the influence of dust emission on the *JHK* spectra, we give the equivalent widths of prominent emission lines estimated from the observed spectra in Table 3. The 1σ errors are ~6–7 per cent of the EW for the He I line at 1.945 µm. For the rest of the lines they are $\leqslant 5$ per cent. Assuming that the fluxes within the emission

---

[1] http://star.pst.qub.ac.uk/~pvh/

Table 1. Log of spectroscopic observations.

UKIRT + CGS4 (150 line mm^{-1} grating), $R = 4700$

UT date (yyyymmdd.dddd)	JD 245 0000+	Bands/ λ (μm)	Phase	d/a
20001013.3495	1830.85	1.07, 1.1	0.9605	0.5092
20001225.1921	1903.69	1.083	0.9856	0.2506
20001226.2004	1904.7	1.083	0.9860	0.2465
20010318.654	1987.15	1.083	1.0144	0.2507
20010331.6208	2000.12	1.083	1.0189	0.3018

UKIRT + CGS4 (40 line mm^{-1} grating), $R = 800$ in *J* band, $R = 400$ in *H* and *K* bands

| UT date (yyyymmdd.dddd)	JD 245 0000+	Bands/ λ (μm)	Phase	d/a
20010331.6618	2000.16	*J, H, K*	0.0189	0.3020
20010428.6164	2028.12	*J, H*	0.0285	0.4045
20010521.5254	2051.03	*J, H, K*	0.0364	0.4810
20010605.4691	2065.97	*J, K*	0.0416	0.5277
20010613.5553	2074.06	*J*	0.0444	0.5521
20010704.6004	2095.1	*J, H, K*	0.0516	0.6129
20010812.2456	2133.75	*J, H, K*	0.0650	0.7156
20010909.3325	2161.83	*J, H, K*	0.0747	0.7841
20011006.2138	2188.71	*J, H, K*	0.0839	0.8457
20011122.2333	2235.73	*J, K*	0.1001	0.9452
20011226.1985	2269.7	*J, K*	0.1119	1.0115
20020403.6638	2368.16	*J, H, K*	0.1458	1.1816
20020630.3636	2455.86	*J, H, K*	0.1761	1.3104
20020717.5517	2473.05	*J, H, K*	0.1820	1.3335

UKIRT + UIST (*IJ, HK* and short_*J* grisms), $R = 3000$ in short_*J*, $R = 950$ in *IJ* and $R = 800$–1000 in *HK* grism

UT date (yyyymmdd.dddd)	JD 245 0000+	Bands/ λ (μm)	Phase	d/a
20030524.5496	2784.05	short_*J*	0.2893	1.6542
20030524.5640	2784.06	*IJ*	0.2893	1.6542
20030524.5740	2784.07	*HK*	0.2893	1.6542

Mt Abu ($R = 1000$)

UT date (yyyymmdd.dddd)	JD 245 0000+	Bands/ λ (μm)	Phase	d/a
19980508.9457	0942.45	*JHK*	0.6540	1.7620
20001221.575	1900.08	*JH*	0.9844	0.2650
20001222.5658	1901.07	*J*	0.9847	0.2610
20001223.5958	1902.10	*J*	0.9851	0.2570
20010102.5861	1912.09	*J*	0.9885	0.2168
20010103.6090	1913.11	*J*	0.9889	0.2127
20010326.9995	1995.50	*J*	0.0173	0.2836
20010328.9988	1997.50	*J*	0.0180	0.2914
20010402.9167	2002.42	*J*	0.0197	0.3106
20010403.8743	2003.37	*J*	0.0200	0.3145

lines did not change, it is evident from the EWs of those in the 1.25–1.28 μm region that dust formation began between 2001 January 3 and March 26 (orbital phases 0.989 and 0.017). At the time of the 2001 March 26 spectrum, light curves from previous cycles predict contributions (relative to the total flux) by dust emission of 22 per cent in *J*, 55 per cent in *H* and 76 per cent in *K*, i.e. dust-to-wind ratios 0.28, 1.2 and 3.2. These are a strong function of wavelength within the bands, e.g. rising from 0.24 at 1.16 μm to 0.32 at 1.28 μm.
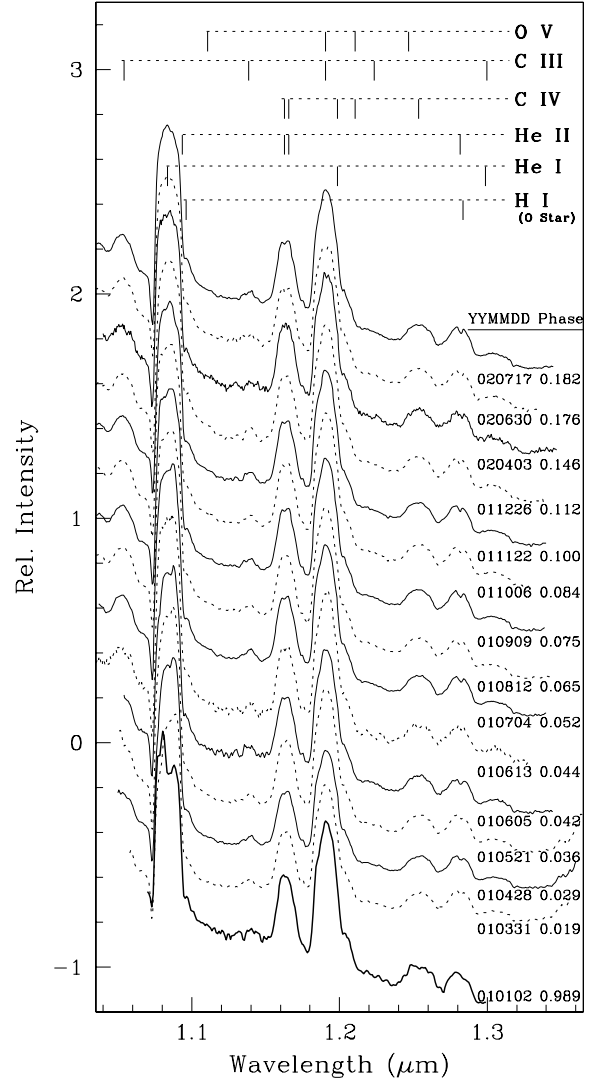
Figure 1. The *J*-band spectra of WR 140 observed using UKIRT and CGS4. Spectra are labelled with the UT date and phase of observation. The *J* spectrum observed using the Mt Abu Telescope on 2001 January 2 is shown at the bottom of the montage for comparison. All spectra are plotted on the same scale with vertical shifts for clarity.

This is consistent with IR light curves from previous cycles (W90), which predict dust emission with a steeply rising spectrum having at phase 0.017 a flux ratio of 0.28 to the stellar wind in the *J* band. The EWs of the 1.166-μm feature are harder to interpret, partly because of increased scatter on their measured strengths and partly because dust emission at this wavelength is about two-thirds that at 1.25 μm (from the model fit to the photometry at this phase in W90). Also, as can be seen in Fig. 1, the slope of the continuum of the *J* spectrum taken in 2001 March 31 is much flatter than that taken on January 2. By the time of the 2003 May observation, when the light curves predict that the dust emission contribution to the total flux had fallen to 10 per cent in the *K* band and below 5 per cent in *J* and *H* bands owing to the cooling of the dust, the slope in the *J* region had returned to that before dust formation. The *H* and *K* spectra show the change in continuum caused by variable amount of dilution due to emission from the dust. The *HK* region shows a nearly flat spectrum during 2001 April when the dust emission was at maximum at these wavelengths, and the spectra became steeper
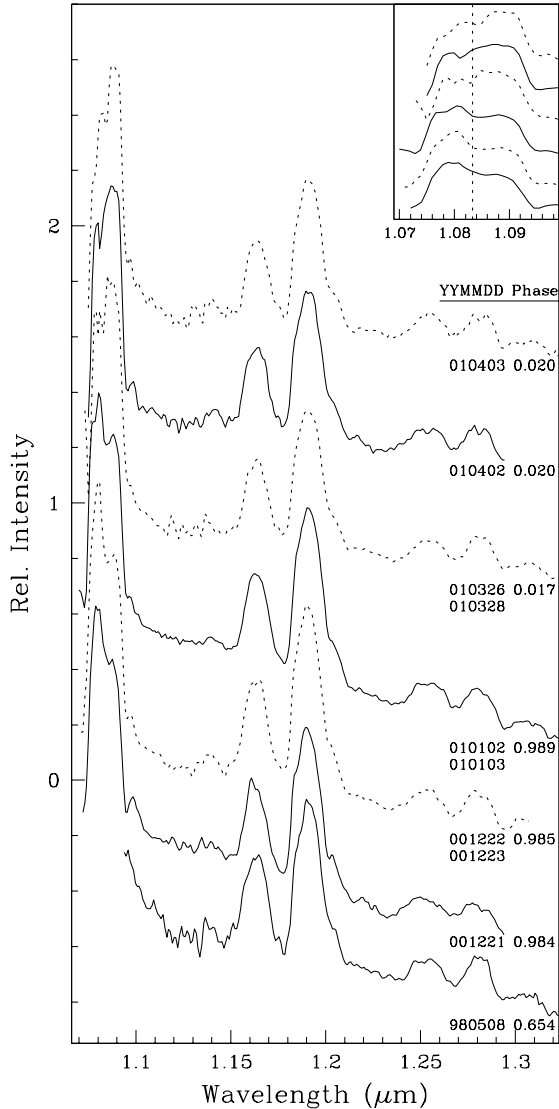
Figure 2. The *J*-band spectra of WR 140 observed using the 1.2-m Mt Abu IR telescope and the NICMOS spectrometer, with spectra observed on consecutive days averaged. The spectra are labelled with the UT date and phase of observation. All spectra are plotted on the same scale with vertical shifts for clarity. The inset shows an expanded view of the evolution of the 1.083-µm He I line. The dashed vertical line shows the central wavelength of the line.

when the dust became cooler. The equivalent widths [Table 3, which includes EWs estimated from the *J* spectrum of Eenens et al. (1991), observed in 1988 with UKIRT and CGS2] of six of these lines are plotted as a function of orbital phase in Fig. 5. This shows the effect of the dilution due to the thermal emission from the dust and the dust cooling. There is a phase lag in the rise of equivalent width with wavelength. This is due to the cooling of the dust and peak emission from the dust shifting to higher wavelengths due to cooling.

4 THE 1.083-µm HeI LINE PROFILE

4.1 The absorption component of the profile

The UKIRT high-resolution spectra covering the He I line ($2s^3S$–$2p^3P$) at 1.083 µm, corrected for the line-of-sight velocity of the WC star at the time of observation, are shown in Fig. 6. This line

and its singlet counterpart at 2.058 µm show P Cygni absorption profiles, from which wind terminal velocities v_∞ of -2650 km s^{-1} (Lambert & Hinkle 1984), -2860 km s^{-1} (Williams & Eenens 1989) and -2900 km s^{-1} (Eenens & Williams 1994) have been measured. These velocities are in good agreement with that (-2900 km s^{-1}) derived from the violet edge of the saturated part of the ultraviolet (UV) C IV P Cygni line profile, v_{black}, by Prinja, Barlow & Howarth (1990), considered to be a better measure of the terminal velocity than the extreme violet edge of the absorption component, $v_{edge} = -3200$ km s^{-1}.

From our high-resolution spectra of the 1.083-µm line, we measured v_{edge}, the velocity at the blue edge of this absorption profile where the absorption merges with the continuum, and v_{abs}, the velocity at the maximum of the P Cygni absorption with respect to the line centre. Two vertical lines are drawn in Fig. 6, at the line centre and at $v = 2840$ km s^{-1}, which is the v_{abs} on 2000 December 25/26, before the periastron passage. Table 4 lists the v_{edge} and v_{abs} measured from the high-resolution spectra. The errors in these velocities are within ±30 km s^{-1}. The core velocities, v_{abs}, are consistent with the measurements of v_∞ and show a smooth variation across the periastron passage, as can be seen well in Table 4 and Fig. 6. The variations in v_{abs} observed in the He I line profile are unlikely to be caused by any He I absorption profile in the wind of the O star. The inset in Fig. 4 shows the *J* spectrum of BS 6736 (9 Sgr), an O4V((f)) star (Walborn 1972), observed with CGS4 in 2001 June. The spectrum of 9 Sgr does not show any significant absorption at this wavelength. We therefore assume that the observed He I absorption occurs in the WC wind material.

As in the UV resonance line profiles, the values of v_{edge} are greater than v_∞, showing a maximum value of ~3320 km s^{-1} in 2000 October and 2001 March and slightly less (~3250 km s^{-1}) in 2000 December and 2003 May. These velocities are close to that measured from the UV profiles (~3200 km s^{-1}) by Prinja et al. (1990) and most probably reflect observation of one or both of the stars through turbulent material near the wind-collision zone.

The depth of the P Cygni absorption component varies considerably, being greater in the 2001 March and 2003 May spectra than in the 2000 October and December spectra. We interpret this in terms of variation of wind material in the sightline to the underlying stellar continuum, which is provided by both the WC7 and O4–5 stars. The greatest absorption was observed in the 2001 March spectra, when our sightline to both stars passed through the He-rich WC stellar wind. This is illustrated in Fig. 7, showing the configurations of the WR 140 system at the epochs of the 1.083-µm spectra. This sketch is in the plane of the orbit; the sightline is from the negative-Y direction and at an angle to the plane of ($\pi/2 - i$), where i is the orbital inclination. On the other hand, the absorption was very much smaller in the 2000 October spectrum. At this phase, the system was nearly at conjunction and we expect the sightline to the O4–5 star to pass through its solar-composition wind (Fig. 7). The configuration in the plane of the axis passing through the two stars and the sightline at the time of the 2000 October observation is shown in Fig. 8. The relatively low He I absorption seen at this phase implies that the angle ψ between the sightline and the axis passing through the two stars is small enough that we observe both stars mostly through the O-star wind, which we assume to provide significantly less He I absorption than the WC wind. Some He I absorption occurs in the WC wind before it hits the interaction region and some in the latter, where turbulence probably accounts for the slightly higher v_{edge} observed at this phase. To interpret the variation of the He I absorption, we must compare the angle ψ, which depends on the orbital elements and phase, with the geometry of the wind interaction region.
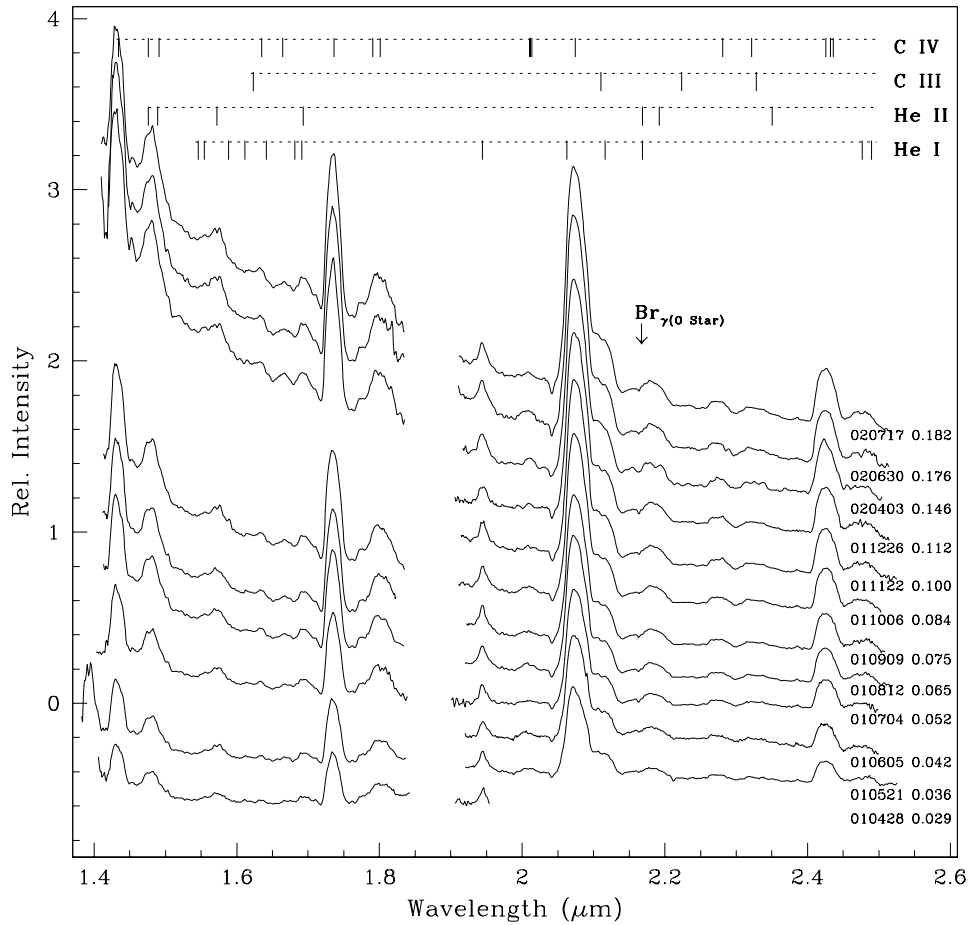
Figure 3. The *H*- and *K*-band spectra of WR 140 observed using UKIRT and CGS4. Spectra are labelled with their UT date of observation and the orbital phase.
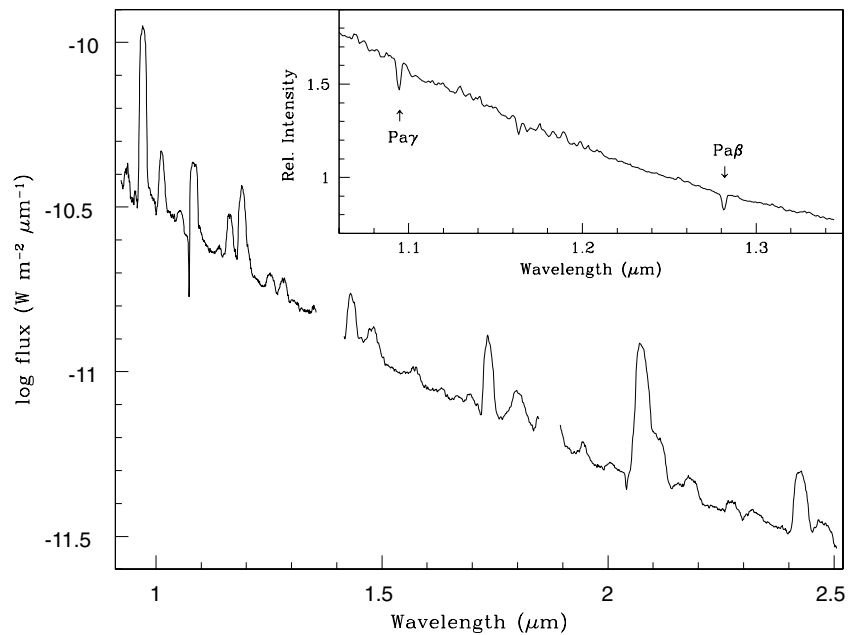
Figure 4. Flux-calibrated *JHK* spectra of WR 140 observed using UKIRT and UIST on 2003 May 24. The inset shows the *J*-band spectrum of the O star BS 6736 (9 Sgr) observed on 2001 June 5. The conspicuous absorption lines in it are Paγ and Paβ at 1.094 and 1.282 μm, respectively.

Table 2. Line identifications, line fluxes, equivalent widths (EW) and full widths at half-maximum (FWHM) from the spectrum observed on 2003 May 24 and dereddened assuming $E(B - V) = 0.6$. The 1σ errors are given in brackets.

λ (μm)	Main contributor	Other probable contributors	Flux (10^{-15} W m^{-2})	EW (Å)	FWHM (km s^{-1})
0.933	C III	0.9347 (He II), 0.936, 0.941 (C III), 0.934 (C IV)	153 (5.7)	−20.3 (0.9)	3160 (67)
0.9529	He I	0.954 (O III)	26 (2)	−3.7 (0.3)	
0.972	C III	0.975, 0.965 (C III), 0.977 (O v)	2431 (5)	−371 (2.1)	
0.987	C IV	0.984 (O v)	122 (13)	−19.2 (2.2)	
1.0126	He II	1.003 (He I, C IV), 1.011–1.023 (C III)	380 (3)	−62 (0.7)	3320 (30)
1.055	C IV	1.055 (C III), 1.053 (C IV)	82 (2.2)	−16 (0.5)	3412 (45)
1.083	He I	1.078 (O v), 1.091 (He I)	558 (3)	−121 (1)	
1.094	He II		44 (2.5)	−10 (1)	
1.1	C IV				
1.139	C IV		30 (2.2)	−7.5 (0.6)	2800 (120)
1.163	He II	1.163 (C IV), 1.164 (C III)	220 (1)	−60 (1)	
1.165	C III	1.168 (He II)			
1.191	C IV	1.188 (C IV), 1.191 (O v)	424 (2.5)	−124 (1)	
1.199	C III	1.197 (He I)			
1.205	O v	1.211 (C III)	47 (3)	−14 (1.5)	
1.226	C IV		7.3 (1)	−2.3 (0.3)	
1.247	O v		66 (1.4)	−23 (1)	
1.255	C III	1.253 (He I), 1.256 (C III), 1.258, 1.261 (C III), 1.255 (O v)			
1.282	He II	1.279, 1.285 (He I), 1.277 (C IV)	70 (1.3)	−27 (0.6)	3600 (30)
1.298	C IV	1.307 (C IV), 1.297 (He I)	21.8 (2.3)	−9 (1)	
1.435	C IV	1.434 (C IV)	140 (3)	−78 (1.8)	3637 (85)
1.454	C III		22 (5)	−13 (3)	
1.476	He II	1.473 (C III), 1.47 (O v)	88 (2.1)	−55 (2)	
1.491	C IV	1.489 (He II)			
1.547	He I	1.547, 1.551 (O IV)	5.5 (0.7)	−4 (0.6)	
1.552	He I				
1.572	He II		27 (0.7)	−21 (0.5)	
1.588	He I	1.58–1.59 (O v)			
1.635	C II	1.635 (O v)	8.5 (0.8)	−7.5 (0.7)	2700 (225)
1.641	He I				
1.664	C IV		10.7 (0.7)	−9.8 (0.7)	
1.693	He II	1.712 (C IV), 1.699 (O v)	25 (1)	−24.8 (1)	
1.701	He I				
1.736	C IV	1.736, 1.737 (C IV)	148 (0.5)	−152 (0.5)	3240 (25)
1.785	C II	1.790 (C IV)	83 (3)	−92 (3)	
1.801	C IV	1.814 (He I), 1.819 (C IV), 1.820 (C II)			
1.944	He I		13.5 (0.7)	−19.5 (1)	2530 (85)
2.012	C IV	2.010 (C IV)	6.0 (0.6)	−9.5 (0.95)	
2.059	He I		284 (3.4)	−493 (7)	
2.071	C IV	2.080 (C IV)			
2.107	C IV	2.108 (C III)	71 (1.2)	−130 (2.5)	
2.113	He I				
2.122	C III	2.139 (C III)			
2.150	He I		7.3 (0.8)	−13.9 (1.4)	
2.165	He I, He II	2.161 (He I, C II), 2.274 (C II)			
2.189	He II		24 (1.4)	−47 (3)	
2.278	C IV		10 (1)	−23.4 (2.3)	3080 (155)
2.318	C IV	2.314 (He II)	13 (0.7)	−31 (1.6)	
2.325	C III	2.328, 2.371 (C IV)			
2.347	He II				
2.423	C IV		65 (0.7)	−175 (1.9)	
2.429	C IV	2.426 (C IV)			
2.433	C IV	2.432 (O v)			
2.473	He I	2.472 (He I), 2.470 (O v)	22 (0.8)	−62 (2.6)	
2.486	He I				

Table 3. Equivalent widths of emission lines.

Date (yyyymmdd)	Phase	1.165 EW	1.255 EW	1.282 EW	1.435 EW	1.736 EW	1.944 EW	2.43 EW
19880715	0.4176	−55	−29.44	−30.3	−78.6			
19980508	0.6541	−66.8	−27.6	−38.		−163.0		
20001221	0.9844	−57.0	−35	−33				
20001223	0.9851	−68.9	−24.0	−28.0				
20010102	0.9885	−62.4	−35.4	−30.3				
20010103	0.9889	−55.0	−30.1	−36.9				
20010326	0.0173	−50.1	−21.4	−24.4				
20010328	0.0179	−49.8	−20.7	−26.2				
20010331	0.0189	−47.8	−19.5	−22.0				
20010402	0.0197	−55.0	−26.6	−29.0				
20010403	0.0200	−56.2	−24.4	−26.7				
20010428	0.0285	−49.4	−20.6	−22.4	−37.9	−60.7		
20010521	0.0364	−58.2	−22.7	−26.8	−44.5	−73.0	−13.4	−40.2
20010605	0.0416	−57.2	−21.8	−24.0			−12	−47.6
20010613	0.0444	−50.0	−25.2	−28.6				
20010704	0.0516	−59.9	−23.8	−27.7	−51.0	−92.0	−14.0	−50.9
20010812	0.0650	−56.3	−24.2	−27.1	−51.9	−104.0	−15.8	−65.6
20010909	0.0747	−57.1	−24.0	−28.0	−55.8	−110.0	−16.4	−69.1
20011006	0.0839	−59.9	−23.9	−28.0	−59.7	−112.5	−17.9	−79.0
20011122	0.1001	−58.2	−24.3	−27.8			−15.6	−90.0
20011226	0.1119	−61.4	−25.1	−29.6			−15.8	−94.3
20020403	0.1458	−58.5	−25.3	−31.2	−62	−125.6	−21.6	−108.5
20020630	0.1761	−56.7	−26.6	−30.3	−65	−131.8	−21	−126.5
20020717	0.1820	−58.4	−27.1	−31.9	−64.7	−135.2	−20.3	−131.0
20030524	0.2893	−63.1	−23	−26.1	−76.7	−148.8	−24.2	−170.6

Both sketches show the contact discontinuities separating the winds. These are defined as the surfaces where the ram pressures of the stellar winds balance, and depend on the wind-momentum ratio

$$\eta = (\dot{M}v_\infty)_O/(\dot{M}v_\infty)_{WR}. \qquad (1)$$

The surface wraps around the star having the lower wind momentum, the O star, on account of its lower mass-loss rate. It has a bow towards the WC star and tends towards a 'cone' on the other side of the O star. Where the orbital motion is slow compared with the stellar wind, the surface is symmetric about the axis joining the WC and O stars. In the case of WR 140, this holds for most of the orbit, except near periastron, when the orbital motion is great enough to cause the interaction region to trail behind the axis at large distances from the stars (Fig. 7). Here, we are concerned with absorption in the winds, which occurs close to the stars, and we will ignore the azimuthal 'twisting' of the interaction regions. Analytical formulae for the form of the contact discontinuity are given by Eichler & Usov (1993) and Cantó, Raga & Wilkin (1996). For comparison with the angle ψ, we use the opening semi-angle θ of the 'cone' given by Eichler & Usov (1993):

$$\theta \simeq 2.1\left(1 - \tfrac{1}{4}\eta^{2/5}\right)\eta^{1/3}. \qquad (2)$$

The angle ψ is given by

$$\cos(\psi) = -\sin(i)\sin(f + \omega), \qquad (3)$$

where f is the true anomaly and ω the argument of periastron. We used the value of ω determined by Marchenko et al. (2003) and their orbital elements to calculate f for each observation. Only the inclination, i, is unknown.

Setia Gunawan et al. (2001) derived $i = 38°$ from the redshifted absorption components of the C IV and Si IV resonance lines observed in an *IUE* spectrum observed at phase 0.01 and near inferior conjunction (O star behind) on their orbital elements. The new orbital elements of Marchenko et al. (2003), however, make a significant difference to the expected configuration of the binary system, which is shifted to about 45° after conjunction at the time of this crucial *IUE* observation, so that it no longer usefully constrains the inclination. Accordingly, we calculated ψ for a range of inclinations for the phase of each observation.

The strong absorption in 2001 March and weak absorption in 2000 October do not greatly constrain θ, but the intermediate observations, on 2000 December 25 and 26 and 2003 May, are particularly valuable. The December spectra concur in showing an absorption feature as weak as that in the October spectrum, indicating that we were still observing the O star through the O star wind. This allows us to set a lower limit on the 'cone' angle θ, which increases with falling inclination. This is illustrated in Fig. 9. Soon after the December observations, the contact discontinuity between the winds swept through our sightline, which then passed through the WC stellar wind, accounting for the high absorption observed in the 2001 spectra when the 'cone' was directed away from us. By the time of the 2003 observation, the He I absorption was still strong, indicating that the 'cone' edge had not yet crossed our sightline, setting an upper limit on θ, again depending on the inclination (Fig. 9).

Thus, θ is fairly tightly constrained, and our observations rule out values around 36° (Eichler & Usov 1993) derived from the wind-momentum ratio, η, given by the mass-loss rates and terminal velocities from W90. This implies that the momentum of the O star wind had been underestimated or that of the WC star overestimated. There is little scope for changing the values v_∞ for the two stars, which come from observations. The mass-loss rate for the O star $(1.8 \times 10^{-6} \, M_\odot \, yr^{-1})$ was adopted from average values (Prinja et al. 1990), while that of the WC star $(5.7 \times 10^{-5} \, M_\odot \, yr^{-1})$ was derived
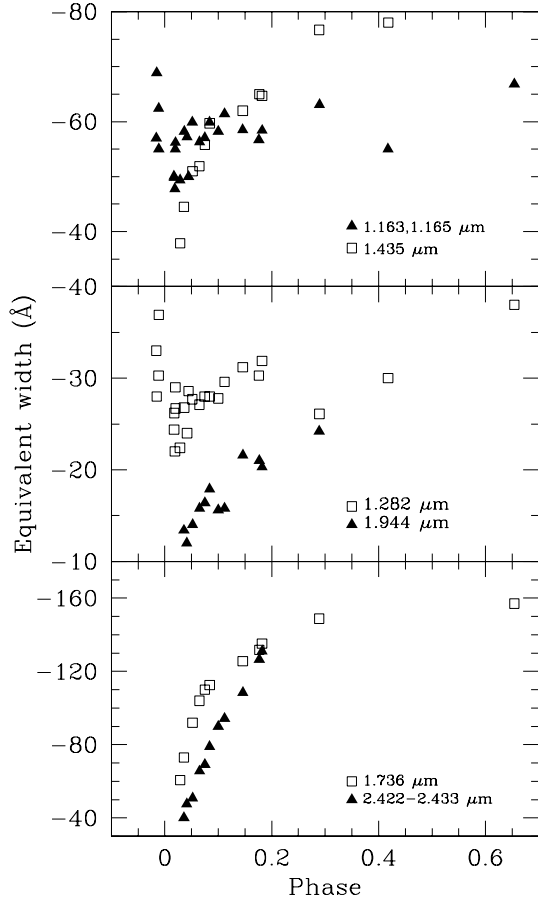
Figure 5. The variation of equivalent width of different emission lines due to dust formation and cooling.

from the 5-GHz flux density at radio minimum, with allowance for the contribution from the wind of the O star. We cannot rule out an approximately three-fold higher mass-loss rate for the O star but note that the value adopted by W90 is supported by recent determinations [1.63×10^{-6} M$_\odot$ yr^{-1} for the O4V((f*)) star HD 303308 and 1.28×10^{-6} M$_\odot$ yr^{-1} for the O5V((f)) star HD 15629 (Repolust, Puls & Herrero 2004)]. We therefore believe that the WC star's mass-loss rate was overestimated because its wind is clumped. A clumped wind with a volume filling factor 0.1 (Dessart et al. 2000) would have a mass-loss rate a factor of $\sqrt{10}$ lower, yielding $\eta = 0.10$ and $\theta = 50°$. This is consistent with the limits set by our He I observations, and will be adopted here.

4.2 The emission component of the He I line

The He I line at 1.083 μm is a very good tracer of colliding-wind phenomena in massive binaries (Stevens & Howarth, 1999). It forms in the asymptotic region of the WR wind and thus it becomes sensitive to wind interactions, which can be observed from additional spectroscopic features on its normally flat top. Eenens & Williams (1994) observed a flat-topped 1.083-μm He I line profile from WR 140 with UKIRT and CGS2 at a resolution of $R = 637$ on 1990 June 20 (corresponding to orbital phase $\phi = 0.66$) although subpeaks were observed from some other WC stars. Reobservation of WR 140 with UKIRT on 1991 October 19 ($\phi = 0.83$) confirmed the absence of structure on the flat top of the 1.083-μm line profile. Yet, by $\phi = 0.96$, the phase of our first high-resolution ($R = 4700$)

UKIRT observation, a conspicuous subpeak had appeared at the short-wavelength end of the profile (Fig. 6). We interpret the appearance of this new emission feature in the intervening 0.13P as evidence of increased interaction of the WC and O type winds as the stars moved closer to each other in their orbit. Between phases 0.83 and 0.96, the separation of the stars decreased from 1.28a to 0.5a, so that the density of undisturbed winds having an r^{-2} density distribution would have increased by a factor of 6.5.

The next high-resolution UKIRT spectra observed on 2000 December 25 and 26 show the subpeak to have strengthened by a factor of $\simeq 2.5$ (Table 4). Corroboration of the presence of the subpeak comes from the $R = 1000$ Mt Abu J-band spectra (Fig. 2) observed on December 21–23. The subpeak was still present on the short-wavelength end of the profile on 2001 January 2–3 (Fig. 2), after which WR 140 was too close to the Sun for us to observe. When WR 140 was again observable in 2001 March, both the UKIRT high-resolution and the Mt Abu spectroscopy showed that the subpeak had shifted to the red end of the profile. We can also track the subpeak in the J-band UKIRT spectra (Fig. 1): the subpeak is visible at the red end of the profile in the 2001 April–July spectra (apart from June 13, which has poor S/N), weakening, broadening and moving back to the centre of the profile in the August–November spectra. It may still be present in the subsequent spectra, which do not show flat-topped profiles. By the time of our next high-resolution spectrum, in 2003 May (Fig. 6), the profile was flat-topped and the subpeak had gone. The structure on the 1.083-μm He I profile is present for only a small fraction of the period, but apparently a larger fraction than the structures analogous to our subpeaks on the 5696-Å C III and 5896-Å He I lines observed by Marchenko et al. (2003).

Marchenko et al. (2003) found that the strengths of the structures on the 5696-Å C III and 5896-Å He I lines varied with the separation of the binary components more steeply than the $1/d$ dependence expected. We have fewer measurements, but it seems that the 1.083-μm line behaves similarly. As noted above, the flux in the subpeak increased by a factor of $\simeq 2.4$ between our 2000 October and December observations while the reciprocal separation, a/d, increased by a factor of 2.05. These spectra were observed before dust formation began and were calibrated with lower-resolution spectrum and photometry. The flux calibration of the 2001 March spectra, observed when there was a contribution from heated dust to the continuum, is less certain, being based on a magnitude, $J = 5.26$, taken for these phases from the J-band light curve of W90 and corrected for the thermal emission from the dust. However, it seems that the flux in the subpeak is stronger still in 2001 March.

The movement of the subpeak is readily understood, qualitatively at least, in terms of the changing orientation of the wind-collision zone with orbital motion, especially around the time of periastron passage. Fig. 7 shows the configuration of WR 140 with the WC star at the origin and the O star in its relative orbit at the orbital phases of the high-resolution UKIRT spectra. The shock cone, wrapped around the O star, is also shown. The observer is in the negative-Y direction (i.e. the line of nodes is parallel to the X-axis). The high-resolution UKIRT spectra of the 1.083-μm He I line are overplotted on this diagram to demonstrate the evolution of the subpeak on the He I line. Its position shifted in accordance with the motion of the components and the associated orientation of the shock cone with respect to the observer, and intensity, with the separation between the components.

We can develop a simple model assuming that the emitting material flows along a thin shell defined by the contact discontinuity, but recognize that real wind collisions are turbulent, full of instabilities and much more complicated (e.g. Walder & Folini, 2002; Folini &
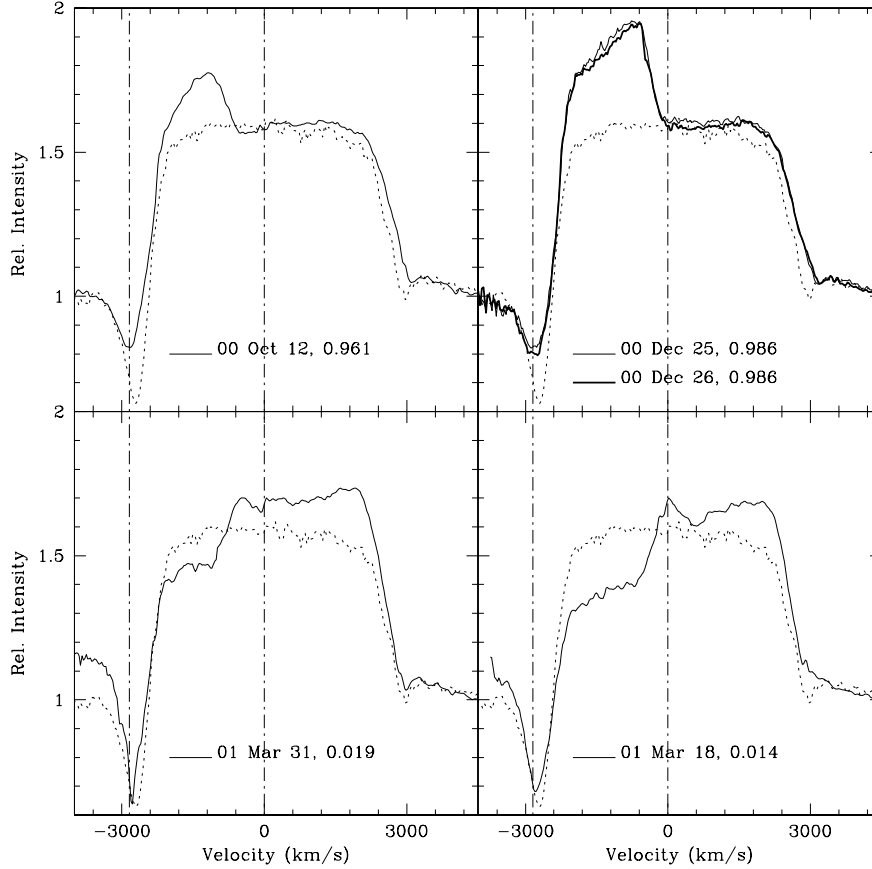
Figure 6. High-resolution spectra of the 1.083-μm He I line observed with UKIRT, corrected for the radial velocity of the WC star, labelled with UT date of observation and orbital phase. The high-resolution spectrum observed on 2003 May 24 is overplotted (dotted) on all the spectra for comparison. The dashed vertical lines are at velocities 0 and $-2840 \, \text{km s}^{-1}$. Variations in both the emission component and the absorption component of the P Cygni profile are evident.

Table 4. Values of v_{edge} and v_{abs} for 1.083-μm spectra and the details of the subpeak.

UT date (yyyymmdd)	Phase	a/d	v_{edge} (km s^{-1})	v_{abs} (km s^{-1})	Subpeak Blue edge[a] (km s^{-1})	Red edge[a] (km s^{-1})	Central vel.[a] (km s^{-1})	Flux (W m^{-2})	P Cyg abs. EW
20001013	0.960	1.96	3316	2860	-2105^b	-526	-1284	3.3×10^{-14c}	2.4
20001225/6	0.986	3.99/4.06	3254	2840	-2167^b	-58	-1056	8.4×10^{-14c}	2.0
20010318	0.014	3.99	3327	2790	-674	$+2521$	$+1060$	$\sim 13.1 \times 10^{-14}$	6.1
20010331	0.019	3.31	3315	2790	-1080	$+2674$	$+801$	$\sim 13.2 \times 10^{-14}$	5.8
20030524	0.289	0.61	3254	2720				0.0	5.2

[a]Velocity with reference to the central wavelength of the WR He I emission line.
[b]Upper limit – the real blue edge will be bluer than this.
[c]Lower limit.

Walder 2002). In Fig. 8, showing a view of the configuration of the system in 2000 October, the shaded area shows the compressed wind material flowing in a thin shell along the contact discontinuity. Cantó et al. (1996) have given a formula for the wind velocity v_s as a function of position on the surface as it accelerates from near the stagnation point between the stars to reach an asymptotic value on the asymptotic region of the contact discontinuity, defined by $\theta_{1\infty}$ subtended at the WC star in the notation of Cantó et al., and approximated by the 'cone' of opening semi-angle θ in the discussion in the previous section. We can resolve v_s into components parallel (v_{axis}) and perpendicular (v_z) to the axis of symmetry. Emission by

material flowing in this shell at any particular phase would have radial velocities in the range

$$\text{RV} = -v_{\text{axis}} \cos(\psi) \pm v_z \sin(\psi), \tag{4}$$

where ψ for that phase comes from equation (3). We do not know from where along the surface the emission arises. If the material near the stagnation point is shock-heated to $\sim 10^7$ K, it seems reasonable to assume that the He recombination occurs downwind and that the emission arises from material on the asymptotic or 'cone' region of the surface, where the velocity has reached its asymptotic, constant value. This becomes analogous to the thin shell model of
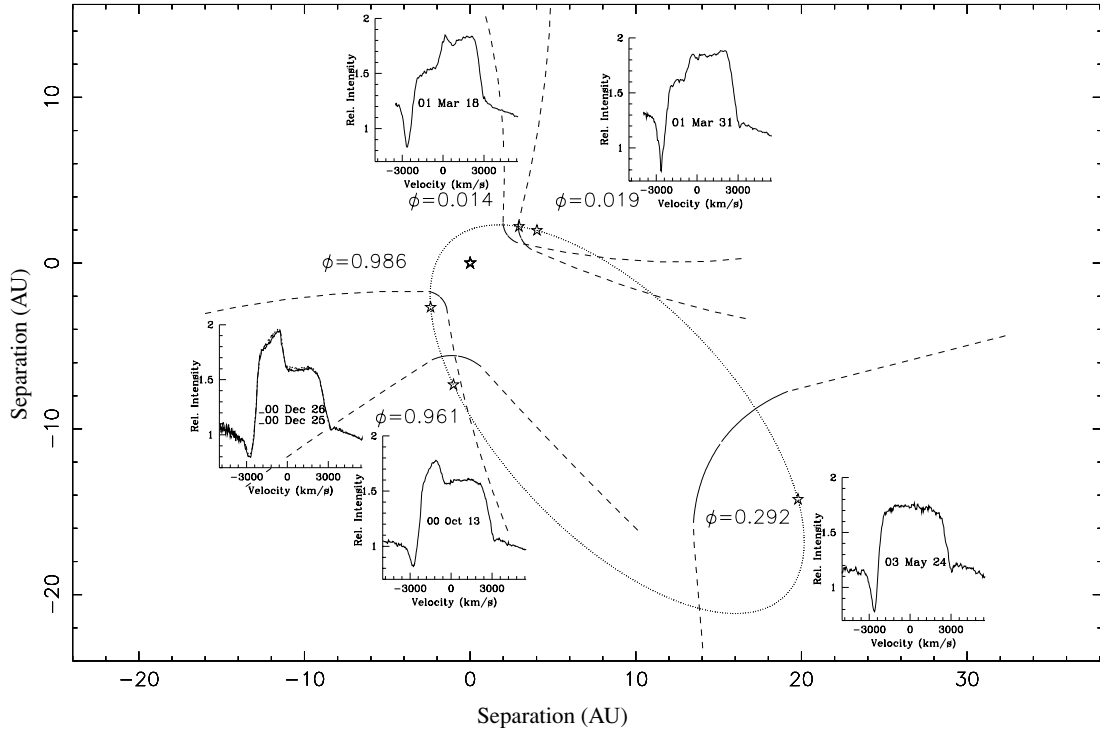
Figure 7. The relative orbit of the O star around the WR star, oriented so that the observer is at negative *Y*. The shape of the contact discontinuity is shown at the phases at which we observed high-resolution 1.083-μm He I spectra. Superimposed on the orbit are the 1.083-μm He I line profiles, which are shown in more detail in Fig. 6.
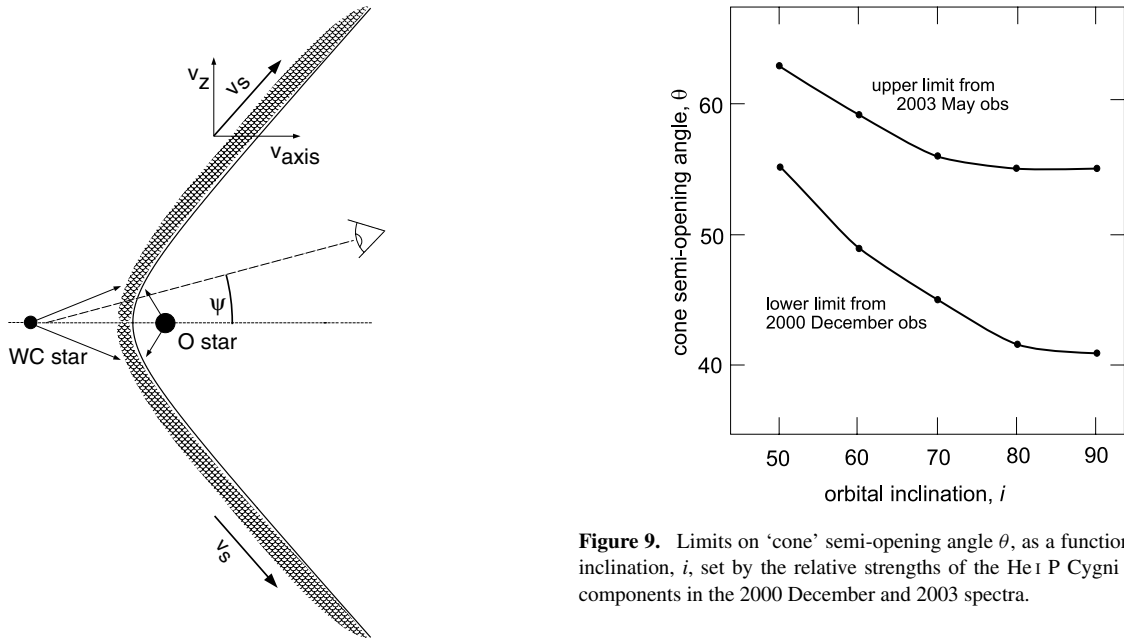

Figure 8. Sketch of the colliding-wind region between the WC and O-type stars in WR 140 in the plane defined by the sightline to the observer and the axis joining the stars. This plane is *not* perpendicular to the orbital plane except at epochs of conjunction. The angle between the sightline and the axis is ψ and the wind interaction region is assumed to be symmetric about this axis. The shaded area represents compressed WC stellar wind material flowing along the contact discontinuity between the two stellar winds. At the time of the 2000 October observation, most of the material (the fraction depending on the unknown orbital inclination) is flowing towards the observer.

Figure 9. Limits on 'cone' semi-opening angle θ, as a function of orbital inclination, *i*, set by the relative strengths of the He I P Cygni absorption components in the 2000 December and 2003 spectra.

Lührs (1997) and Hill, Moffat & St-Louis (2002) except that, instead of solving for the cone angle and flow velocity, we will adopt the value of θ derived above and determine the flow velocity following Cantó et al. (1996, equation 29) from the terminal velocities of the WC and O stars (2860 and 3100 km s^{-1} respectively; W90).

From these, we derived velocity components $v_{\mathrm{axis}} = 1505$ km s^{-1} and $v_z = 1835$ km s^{-1} for our $\eta = 0.10$ surface, which corresponds to $\theta = 50°$. We use these and equation (4) to model the variation of the RV of the centre and extent of the emission from the thin
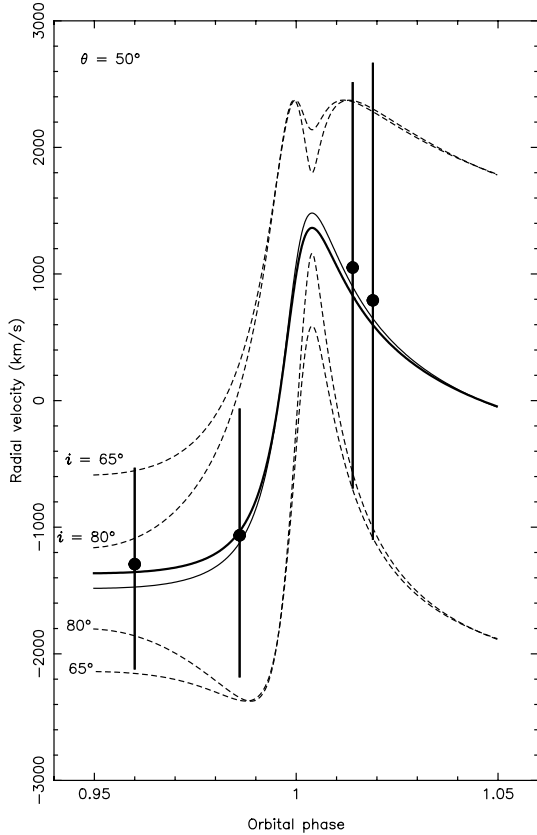
Figure 10. Comparison of variation with orbital phase of observed radial velocities of subpeaks on the 1.083-µm line (vertical bars at phases of observation show extents of the subpeaks, with black circles marking the central velocity) with the model described in the text for two values of orbital inclination. The solid line shows the central velocity, the thicker line for $i = 65°$, and the thinner line for $i = 80°$. The extents of the emission feature for the two values of i are marked with dashed lines, labelled where the model is sensitive to inclination.

shell as a function of phase for different values of the inclination. This is shown for $i = 80°$ and $i = 65°$ in Fig. 10, where the models are compared with the observed velocities of the centre and extent measured from our high-resolution UKIRT spectra.

The agreement is very encouraging: the simple model successfully explains the movement of the centre of the line and reasonably approximate its width. From comparison with the October observation, we suggest that the orbital inclination is close to $i = 65°$. The discrepancies at the blue edges of the pre-eclipse subpeaks are expected since we are not able to measure accurately the 'real' blue edge of the subpeak before the periastron passage since it overlaps the steep, P Cygni absorbed, region of the profile, which also results in an underestimation of the flux in the subpeak during these phases. Given the uncertainties, we have not attempted a formal solution for inclination. Tests showed that the model is not very sensitive to θ in the range set by the absorption components (Fig. 9).

5 DISCUSSION

The flux in the subpeak (Table 4) on the He I profile is a significant source of cooling for the shock-heated material, exceeding the 2–6 keV X-ray flux (2.5×10^{-14} W m^{-2}) observed with *EXOSAT* near the time of the 1985 periastron passage (W90) or the 1–10 keV flux

(2.4×10^{-14} W m^{-2}) observed with *ASCA* by Koyama et al. (1994) in 1993 June, shortly after the following periastron passage.

Koyama et al. (1994) also noted that their X-ray flux was not significantly different from that observed with *Ginga* in 1987 (Koyama, Kawada & Takano 1990), at a phase when the orbital separation was $\simeq 4$ times that of their 1993 observation. They pointed out that this, and the *EXOSAT* results, showed no convincing evidence that the X-ray flux above 2 keV, which should be relatively unaffected by interstellar or orbitally modulated circumstellar extinction, varied systematically with orbital separation. This was in contrast to the $1/d$ dependence expected theoretically for the X-ray luminosity of WR140 (Stevens, Blondin & Pollock 1992), on the basis that the shocked winds were close to adiabatic because the cooling time of the shocked X-ray-emitting material was long compared with the characteristic flow time.

This discrepancy was studied further with additional *ASCA* data by Zhekov & Skinner (2000) and Pollock, Corcoran & Stevens (2002). Both studies sought to adjust the orbital elements of WR 140 derived by W90 to recover the $1/d$ dependence for the X-ray fluxes, either reducing the eccentricity to $e = 0.55$ or bringing forward T_0 by $0.025P$ (72 d). The proposed lower eccentricity is effectively ruled out by confirmation of the high eccentricity in the more recent orbital solutions by (Setia Gunawan et al. 2001, $e = 0.87$) and (Marchenko et al. 2003, $e = 0.881$). From the variations of the 1.083-µm He I line profile observed around the periastron passage (Figs 1, 2 and 6), we see that the subpeak remained blueshifted until 2001 January 2 and had moved to the red end of the profile by March 18. If we are correct in interpreting this movement as a change of the orientation of the wind-collision region moving with the stars in their orbits, then quadrature and periastron passage must have occurred after January 2. This is consistent with the predictions of T_0 of 2001 February 20 (W90) or February 6 (from elements by Marchenko et al.) but rules out the 72-d shift to December 10 proposed by Zhekov & Skinner. (Setia Gunawan et al. also proposed moving T_0 forward, by 104 d relative to the elements of W90, but with a relatively large uncertainty, 117 d, which does not constrain our solution.)

We propose instead that the X-ray flux departs from a $1/d$ dependence because the shocked WC wind is not totally adiabatic during periastron passage as a consequence of significant additional cooling in the He I subpeak.

6 CONCLUSIONS

Infrared spectroscopy of WR 140 during and after its 2001 periastron passage showed dilution of the emission lines consistent with the formation of circumstellar dust between 2001 January 3 and March 26, phases 0.989 and 0.017. The He I 1.083-µm line showed a strong P Cygni profile. Variation of the strength of the absorption component measured from high-resolution spectra was interpreted in terms of the passage of different parts of the colliding-wind structure in our line of sight to the two stars. This allowed us to set fairly tight limits on the opening half-angle of the 'cone' modelling the interaction region: $\theta = 50° \pm 8°$. This, in turn, indicated a wind-momentum ratio $\eta = 0.10$, significantly higher than the $\eta = 0.034$ found from the mass-loss rates and terminal velocities of the WC7 and O components. We suggested that the mass-loss rate of the WC7 star, 5.7×10^{-5} M$_\odot$ yr^{-1}, derived from the 5-GHz flux density at radio minimum, was overestimated because the wind is clumped.

At phases ($\Delta\phi \simeq 0.1P$) close to periastron passage, the normally flat-topped emission component of the 1.083-µm line showed the

appearance of a subpeak, which moved from the blue to the red end of the profile during periastron. The evolutions of the position and width of the subpeak were found to be reasonably consistent with the flow of the emitting material along the surface of the interaction region modelled by a cone having $\theta = 50°$. The maximum radiative flux in the subpeaks is greater than the 1–10 keV X-ray flux at periastron and is a significant source of cooling of the shocked WC wind. We suggest that the shocked WC wind is not totally adiabatic near periastron, thereby accounting for the departure of the X-ray flux from the previously expected $1/d$ dependence and, as suggested by Marchenko et al. (2003), allowing dust formation.

REFERENCES

Cantó J., Raga A. C., Wilkin F. P., 1996, ApJ, 469, 729
Dessart L., Crowther P. A., Hillier D. J., Willis A. J., Morris P. W., van der Hucht K. A., 2000, MNRAS, 315, 407
Eenens P. R. J., Williams P. M., 1992, MNRAS, 255, 227
Eenens P. R. J., Williams P. M., 1994, MNRAS, 269, 1082
Eenens P. R. J., Williams P. M., Wade R., 1991, MNRAS, 252, 300
Eichler D., Usov V., 1993, ApJ, 402, 271
Folini D., Walder R., 2002, in Moffat A. F. J., St-Louis N., eds, ASP Conf. Ser. Vol. 260, Interacting Winds from Massive Stars. Astron. Soc. Pac., San Francisco, p. 605
Hill G. M., Moffat A. F. J., St-Louis N., 2002, MNRAS, 335, 1069
Koyama K., Kawada M., Takano S., 1990, PASJ, 42, L1
Koyama K., Maeda Y., Tsuru T., Nagase F., Skinner S., 1994, PASJ, 46, L93
Lambert D. L., Hinkle K. H., 1984, PASP, 96, 222
Lührs S., 1997, PASP, 109, 504
Marchenko S. V. et al., 2003, ApJ, 596, 1295
Monnier J. D., Tuthill P. G., Danchi W. C., 2002, ApJ, 567, L137
Panov K. P., Dinko D., 2002, Inf. Bull. Variable Stars, 5177
Panov K. P., Altmann M., Seggewiss W., 2000, A&A, 355, 677
Pollock A. M. T., Corcoran M. F., Stevens I. R., 2002, in Moffat A. F. J., St. Louis N., eds, ASP Conf. Ser. Vol. 260, Interacting Winds from Massive Stars. Astron. Soc. Pac., San Francisco, p. 537
Prinja R. K., Barlow M. J., Howarth I. D., 1990, ApJ, 361, 607
Repolust T., Puls J., Herrero A., 2004, A&A, 415, 349
Setia Gunawan D. Y. A., van der Hucht K. A., Williams P. M., Henrichs H. F., Kaper L., Stickland D. L., Wamsteker W., 2001, A&A, 376, 460
Stevens I. R., Howarth, I. D., 1999, MNRAS, 302, 549
Stevens I. R., Blondin J. M., Pollock A. M. T., 1992, ApJ, 386, 265
Vreux J.-M., Andrillat Y., Biémont E., 1990, A&A, 238, 207
Walborn N. R., 1972, AJ, 77, 1972
Walder R., Folini D., 2002, in Moffat A. F. J., St. Louis N., eds, ASP Conf. Ser. Vol. 260, Interacting Winds from Massive Stars. Astron. Soc. Pac., San Francisco, p. 595
Williams P. M., 1995, in van der Hucht K. A., Williams P. M., eds, Proc. IAU Symp. 163, Wolf–Rayet Stars, Binaries, Colliding Winds, Evolution. Kluwer, Dordrecht, p. 335
Williams P. M., Eenens P. R. J., 1989, MNRAS, 240, 445
Williams P. M., van der Hucht K. A., van der Woerd H., Wamsteker W. M., Geballe T. R., Garmany C. D., Pollock A. M. T., 1987, in Lamers H. J. G. L. M., de Loore C. W. H., eds, Instabilities in Luminous Early Type Stars. Dordrecht, Reidel, p. 221
Williams P. M., van der Hucht K. A., Pollock A. M. T., Florkowski D. R., van der Woerd H., Wamsteker W. M., 1990, MNRAS, 243, 662 (W90)
Zhekov S. A., Skinner S. L., 2000, ApJ, 538, 808

This paper has been typeset from a TEX/LATEX file prepared by the author.